metals

Article

Durability of Single Lap Friction Stir Welded Joints between S355-J0 Steel and AA5083 Aluminum Alloy–Mechanical Tests

Borsellino Chiara *, **Federica Favaloro** and **Guido Di Bella**

Department of Engineering, University of Messina, Contrada di Dio 1, 98166 Messina, Italy; federica.favaloro@unime.it (F.F.); guido.dibella@unime.it (G.D.B.)
* Correspondence: chiara.borsellino@unime.it

Abstract: This study aims to investigate a friction stir welded joint between steel and aluminum alloy. FSW is nowadays one of the most interesting joining techniques due to the possibility of connecting materials and thicknesses that are difficult or impossible to weld with traditional techniques. The main advantage is that materials are not affected by thermal cycle problems during solidification and cooling, and the absence of fumes and pollution during the process favors the quality of the welded joint. The life of metal joints could be greatly reduced in a corrosive environment since the less noble material will tend to increase its corrosion rate, while the nobler one will reduce its electrochemical dissolution. Accelerated aging tests (i.e., salt fog test) are used to estimate the lifetime of metal joints in highly aggressive environments. The aim of the present work is to evaluate the durability at a long aging time in the salt spray test (according to ASTM B117) of carbon steel/aluminum alloy joints, obtained by FSW. In this first part, mechanical test results are reported. A deep metallographic and chemical investigation is going to be reported in part two. The current research work investigates the welding direction and residence time in the salt spray chamber. The breakage of all tested samples, evaluated after the tensile tests were carried out, always occurs at the interface of the joint, regardless of the change of direction of the weld on the advancing or retreating side. The welding direction influences the breakage of the joint only before the aging treatment. Specifically, specimens produced in advance are characterized by increased joint strength. On the other hand, the factor that influences the performance of the joints is the exposure time where, starting from the first point of aging, i.e., after two months, there is a decrease in the maximum load of 40%, and the effect of corrosion leads to a significant deterioration of the weld which remains almost similar until the last point of aging.

Keywords: joining; FSW; shipbuilding; aluminum; steel; aging tests; salt spay

Citation: Chiara, B.; Favaloro, F.; Di Bella, G. Durability of Single Lap Friction Stir Welded Joints between S355-J0 Steel and AA5083 Aluminum Alloy–Mechanical Tests. *Metals* **2024**, *14*, 137. https://doi.org/10.3390/met14020137

Academic Editor: Masahiro Fukumoto

Received: 13 December 2023
Revised: 18 January 2024
Accepted: 21 January 2024
Published: 23 January 2024

1. Introduction

The EU is committed to carbon neutrality by 2050 due to the recent adoption of the European Climate Law. Energy consumption and CO_2 emissions are directly affected by the low weight of the transportation body. A multi-material body is crucial for reducing CO_2 emissions as it allows for a very low weight and decreased production costs [1]. To reach this goal, it is possible to use new materials, new combinations of bimetallic joints, or suitable advanced methods of material joining. The combination of metallic materials with different electro potentials can lead to an increased risk of galvanic corrosion. The joining of different materials, such as welding aluminum and steel, results in ideal conditions for bimetallic corrosion at the direct contact point [2]. The quality deterioration and rapid failures of marine constructions due to low corrosion resistance are significant problems that decrease human safety and reliability [3]. Welded marine structures are constantly exposed to the corrosive effects of seawater and high-humidity environments [3].

The corrosion of joints between steel and aluminum welded using the FSW process is a well-known and significant issue in the field of materials engineering and welding. This phenomenon can lead to severe structural damage and compromise the integrity of the joints. In general, FSW is known for providing high-strength joints, but their durability in a marine environment can be influenced by various factors, in particular, the FSW process can affect the ease with which the corrosion process occurs at the joint between these two types of metals. However, even if the problems related to the durability in the aggressive environment of different materials are industrially known [4], in the literature, only a few works aimed to better relate aspects of corrosion degradation with the mechanical behavior of the joints are reported.

The main effects are as follows:

Formation of composite joints: FSW creates a joint composed of both metals, steel, and aluminum. This joint has a unique microstructure that can influence the susceptibility to corrosion. For example, the transition zone between the two metals, known as the "stir zone", may have different characteristics that affect chemical reactivity. Differences in the galvanic potential: The formation of composite joints between steel and aluminum creates an area where differences in electric potential between the two metals can promote galvanic corrosion. The joint itself often serves as a preferential site for the initiation of corrosion, with aluminum acting as the anode and steel as the cathode in a galvanic reaction. The higher corrosion current density is generated in the welded zone due to the occurrence of galvanic corrosion [5].

Precipitation of intermetallic compounds: In composite joints between steel and aluminum, intermetallic compounds can form due to the interdiffusion of metals during welding. These intermetallic compounds may have a greater susceptibility to corrosion than the base metals, increasing the risk of corrosion damage. Sachindra et al. reported that "the grain structure of each zone depends on the dynamic recrystallization and heat input. However, dynamic recrystallization is more dominating factor compared to the heat input in the stir zone and thus leads to the more refined grains in the stir zone. Like grain structure, distribution of harder material over the aluminum in the weld zone also plays a great role in deciding the joint quality. The formation of intermetallics is also crucial for dissimilar joining. The interface of the Al to non-Al metallic combinations is sensitive to the formation of intermetallics due to the diffusion of the materials to be joined. However, the thickness of the intermetallics is thinner in FSW of dissimilar materials compared to fusion welding. The thickness of the intermetallic compound in the interfacial zone has adverse effects on the tensile strength of the joint. However, the tensile strength of FSW Al to Non-Al metallic combinations is always lower than the aluminum base metals due to the formation of defects and intermetallics" [6,7].

Porosity Effect: The FSW process can create some porosity at the interface between the two materials. These pores can act as preferential sites for the initiation of corrosion, as they facilitate the access of moisture and electrolytes. The results obtained from Zhenglin's research [8] show that the FSW technique significantly reduces porosity in welding. It is believed that the plastic deformation and dynamic recrystallization process developing in FSW was able to exclude porosity in the weld. Moreover, the absence of melting eliminates porosity and hot cracking, problems that have been shown to occur when fusion welding aluminum and its alloys [9].

Welding parameters: Welding parameters influence the microchemistry and, thus, the microstructure of friction welded joints. Among the parameters that determine these changes, we can mention the speed of rotation, the direction of advancement in the advancing or retreating side, the tilt angle, the geometry of the pin and the tool, etc. For Zhan et al. [5], as the rotational speed increases, it increases the average grain size due to severe plastic deformation and high-temperature exposure, and dynamic recrystallization takes place in the nugget zone (NZ), forming fine equiaxed grains. Due to the uneven shear deformation and heat input at different positions in the NZ, different types of texture components are formed and vary with the rotational speed. Depending on the heat input, FSW limits the formation of intermetallics at the Al-to-steel interface because it involves lower temperatures and avoids melting. A higher rotational speed and larger tool offset can be used to modify the overall temperature distribution in the weld [10]. Chen et al. [11]

studied the effects of tool positioning on microstructures formed in the Al-to-steel interface region and reported that when the pin was close to the bottom steel piece, an Al-to-steel reaction occurred, resulting in intermetallic outbursts formed along the interface. When the pin approached the steel, a thin and continued interface intermetallic layer was formed [12]. Sanjay et al. proposed that the weld parameters, like the speed of welding and rotation, control the material flow and, thus, reduce weld defects. The above-discussed parameters are already discussed in many papers, so special attention is given to factors like tool material selection, tool geometry and design, joint configuration, and physical properties of base metals [13]. The welding of dissimilar alloys is influenced by both the shape and the profile of the shoulder [14,15]. Jaia et al. [16] find that the pin geometry influences both the tensile elongation and the value of the breaking load; several authors agree that a spiral pin profile would increase welding effectiveness. Di Bella et al. studied the effect of the tool tilt and the tool was inclined to an angle of 2°. This induces an evident effect on the joint [17].

The evaluation of durability, by accelerated tests, of dissimilar Al/Steel joints has been performed by some authors, but mainly regard other joining techniques but FWS. For example, Wloka et al. [18] studied the corrosion properties of laser beam joints of aluminum with zinc-coated steel, finding that the corrosion tests show that the joining zone has the most negative corrosion potential and is the first to corrode. The degree of corrosive deterioration depends on the cathodic behavior of the adjacent metal. Next to effective cathodes, such as steel or Fe-containing intermetallics, the attack is the most common. The corrosion performance of laser-brazed joints of AA6082 to galvanized steel was studied with three different methods: immersion test, salt spray test, and electrochemical corrosion test by Narsimhachary et al. [19].

Calabrese et al. [20] performed long-term aging tests in critical environmental conditions to evaluate the mechanical durability of aluminum alloy/steel self-piercing riveting (SPR) joints. The experimental results evidenced that the corrosion degradation phenomena significantly influenced the performances and failure mechanisms of the joints.

Le Bozec et al. [4] investigated the corrosion performance and mechanical properties of various joints composed of different material combinations (e.g., high-strength carbon steel, hot-dip galvanized steel, electrogalvanized steel, aluminum alloys 6061 and 5182) using different mechanical joining methods, including adhesive + clinching and clinching alone. They found that hybrid (adhesive + clinching) joints had greater strength than clinching when both types of joints were subjected to corrosion testing prior to a mechanical strength evaluation.

Lim et al. [21] studied the joint strength of dissimilar combinations of AA 7075-T6 and DP 980 sheets welded by friction bit joining (FBJ) for spot joints produced with and without adhesive, using an accelerated laboratory scale corrosion cycle test.

Nevertheless, some studies on the durability of dissimilar Al/steel FSW joints have been performed, but the focus has been on the investigation of immersion corrosion and electrochemical corrosion tests. Kulkarni et al. studied the FSW process, and variables such as the backing plate, the rotation speed of the tool, and traverse speed were varied to obtain a suitable combination of parameters to achieve high corrosion resistance of joints along with satisfactory mechanical properties [22].

Anaman et al. [23] found friction stir butt welded joint of dissimilar aluminum and steel alloys, and the electrochemical corrosion investigation reveals that the FSW joint exhibits a higher corrosion rate compared to the base materials due to the scattered steel fragments and the increase in martensite content and low-angle grain boundaries (LAGBs).

In a previous study, the authors [24] evidenced how, for the connection of steel with aluminum alloy, by varying the direction of welding, the mechanical properties change, proving that this process parameter affects temperatures, deformations, residual stresses, and, consequently, the mechanical properties. The microstructure analyses evidenced that a thin intermetallic compound (IMC) layer at the aluminum and steel interface can be clearly observed due to the rotation effect of the pin, which pulled small pieces of steel from the surface and scattered them on the aluminum surface. By changing the weld side, the quantity and shape of these steel fragments change by affecting the mechanical behavior [20]. So, it is not possible to exclude that the welding direction can affect the durability of the joint. A preliminary test was performed [25] on the same sample before aging and studying the electrochemical behavior (by microcell polarization tests) of the joint shows that the zones formed during the FSW process (stir and heat affected zone) did not negatively affect the corrosion resistance of the joint.

Corrosion in joints between steel and aluminum welded with FSW is a complex problem that requires a combination of technical approaches, such as coatings, material selection, and design, to successfully prevent or mitigate it. Careful management of this issue is crucial to ensure the reliability and durability of structures and components involving these joints. Despite the criticality of the problem, as before pointed out, very few studies on the durability of FSW joints between aluminum and steel can be found in the literature. In this concern, the aim of the present work is to evaluate the effect of the aging time in a salt spray test on the mechanical performances and failure mechanisms of carbon steel/aluminum alloy joints, obtained by FSW.

2. Materials and Methods

In this study, the joining between aluminum and steel was evaluated with materials that are impossible to weld with traditional techniques, and possessing different chemical characteristics. The use of dissimilar materials, in the industrial sector, is carried out to meet all those construction needs where it is necessary to lighten the structures. The friction welded joints were made by joining 6 mm thick AA5083-H111 aluminum alloy sheets, supplied by Media Metalli (Villaricca, Italy), and 5 mm thick S355-J0 steel sheets. Both the materials and the thicknesses were chosen and indicated by the partner company of the project, the Fincantieri shipyard in Palermo (Trieste, Italy), as such materials are employed in their shipyard. AA5083 is a very versatile aluminum alloy, its use is aimed at a multitude of sectors such as railways, automobiles, and ships, but it is not possible to heat treat it. To improve its mechanical characteristics, it is possible to carry out a work hardening treatment through the cold forming technique. The H111 condition was achieved during subsequent operations, such as stretching or leveling. The result is an annealed and slightly hardened alloy (less than H11 hardening). S355-J0 is an unalloyed carbon structural steel suitable for cold forming. It is used in many different fields, from carpentry applications (i.e., naval), to the production of metal structures and tanks, to its use in architecture, etc. J0 means that, at a temperature of 0 °C, the minimum impact energy, is equal to 27 J. The preliminary tests, tensile and microhardness tests, were to evaluate the main properties of aluminum and steel. Tables 1 and 2 show, respectively, the chemical composition and the main mechanical properties of both materials used.

Table 1. Chemical composition of AA5083-H111 aluminum alloy and S355-J0 steel (wt. %).

	Al	Mg	Mn	Si	Fe	Cr	Zn	C	T	Cu	S	P	N	Other
AA5083-H111	Bal.	4.0–4.9	0.4–1.0	<0.4	<0.4	0.05–0.25	<0.25	-	<0.15	<0.1	-	-	-	<0.15
S355-J0	-	-	<1.60	<0.55	-	-	-	<0.20	-	<0.55	<0.03	<0.03	<0.012	-

Table 2. Mechanical properties of AA5083-H111 aluminum alloy (adapted from Ref. [15]) and S355-J0 steel.

	Rm [MPa]	Rp02 [MPa]	A [%]	HV0.1
AA5083-H111	>275	>125	16	82
S355-J0	470–630	355	22	-

The joint was made using a welding speed of 300 mm/min at 400 rpm and with a force control of 30 kN, changing the feeding direction of the tool along the welding line and maintaining the same rotation direction of the tool (clockwise). In Figure 1, the single-lap FSW joint between the aluminum alloy (AA5083-H111) and the steel sheet (S355-J0) is shown. The direction of the tool's rotation is identified as follows: (i) AD, when the advancing side is by the side of the steel (lower plate), and (ii) R, when the retreating side is by the steel side (lower plate).

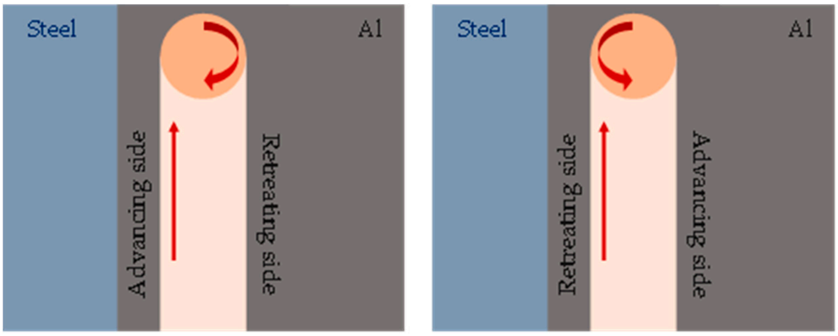

Figure 1. Advancing and retreating sides (adapted from Ref. [24]).

Figure 2 shows the section of the joint where the aluminum and steel subjected to the welding process are highlighted (aluminum/sheet metal interface).

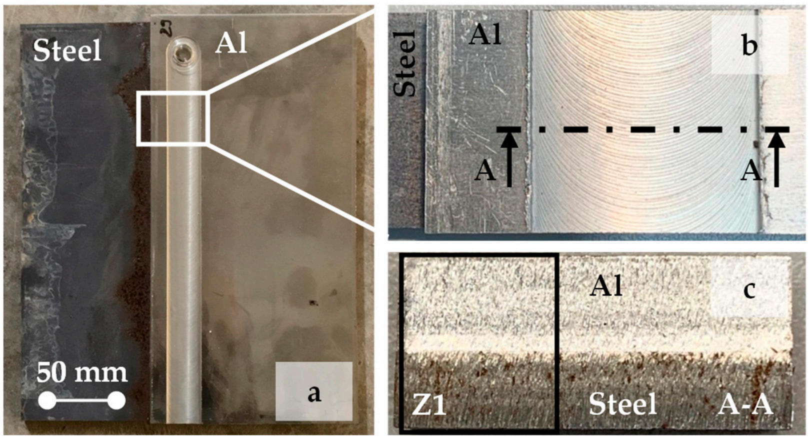

Figure 2. FSW area: (**a**) whole joined structure; (**b**) zoom on the aluminum area involved by the tool, section after cutting, and treated area (mechanical and etching); (**c**) optical microscope image of the steel inclusions (adapted from Ref. [24]).

The salt spray test is an accelerated test method that is commonly used to assess the corrosion resistance of different materials in controlled corrosive environments [26]. The accelerated aging test was realized through the DCTC 600P salt spray chamber, located at the Department of Engineering of Messina, according to ISO 9227 [27] and ASTM B117 [26] standards. The accelerated aging tests were conducted on both types of specimens produced, therefore, in the advancing and retreating side, creating five aging points (from 2 months to 12 months) which, in total, constitute six levels for the "month" factor, also considering the T0 time that constitutes the specimen without aging treatment.

Five aging points were then identified and reported in the following experimental plan (see Table 3), and the mechanical characterization tests were carried out through tensile tests using the Zwick/Roell Z600 tensile machine in the Structures Laboratory of the Engineering Department.

Table 3. Experimental plan salt spray aging—Materials: AA5083–S355-J0.

Parameters:	T0	T1	T2	T3	T4	T5
Months (5 aging points)	2	4	6	8	10	12
Welding Direction (Advancing/Retreating)	AD/R	AD/R	AD/R	AD/R	AD/R	AD/R

The nomenclature used for the samples subjected to the accelerated aging tests is given below; for the specimens obtained through FSW, the wording FSW_AD_N and FSW_R_T_n has been used, where:

- FSW_AD corresponds to the specimen made for FSW on the advancing side.
- FSW_R corresponds to the specimen made for FSW on the retreating side.
- T_n represents the time.

For example, the wording FSW_R_T1 corresponds to the sample made with FSW in the retreating side and tested at time T1, i.e., at two months of accelerated aging. The joints were mechanically characterized through tensile tests, a Zwick/Roell Z600 testing machine with a 600 kN load cell, equipped with a 10 kN load cell, in accordance with UNI EN ISO 12996 [28]. The crosshead rate was set to 1 mm/min. For each configuration (i.e., advancing and retreating), five samples were tested.

3. Results

3.1. Failure Modes

Figure 3 shows the typical failure mode of a joint made for FSW; it is possible to observe the joint area between the steel and the aluminum where the lines produced by the pin during the feed are evident.

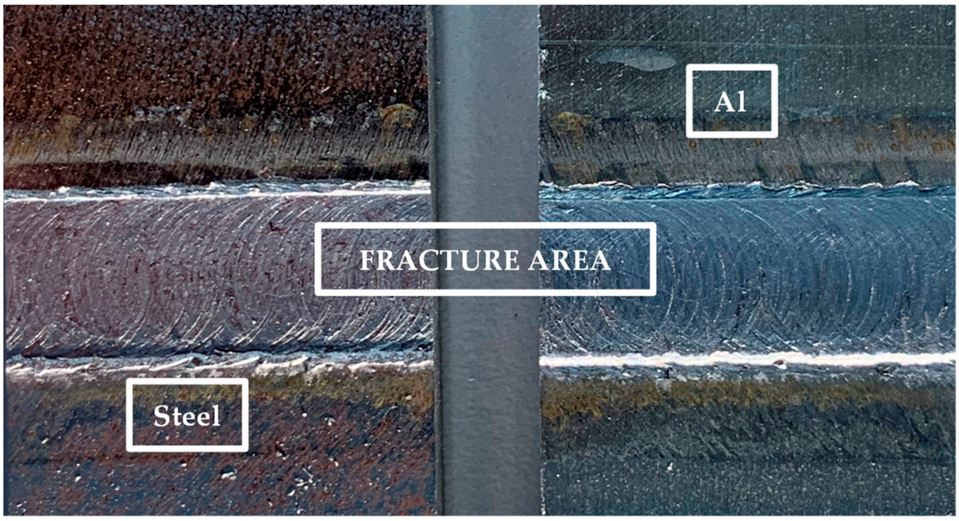

Figure 3. Failure area of an FSW-AD joint.

Figures 4 and 5 show the evolution of the decay of the tested joints due to corrosion, for all investigated aging points. The samples at time T0 are shown, respectively, which correspond to the unaged specimen. Then, T1, T2, T3, T4, and T5 show where the propagation of the corrosion phenomenon is evident as early as time T1, which corresponds to two months of accelerated aging treatment. Corrosion continues as the time spent in the salt spray chamber increases, up to the fifth point of aging and twelve months of aging, where the corrosion products completely cover the external surfaces.

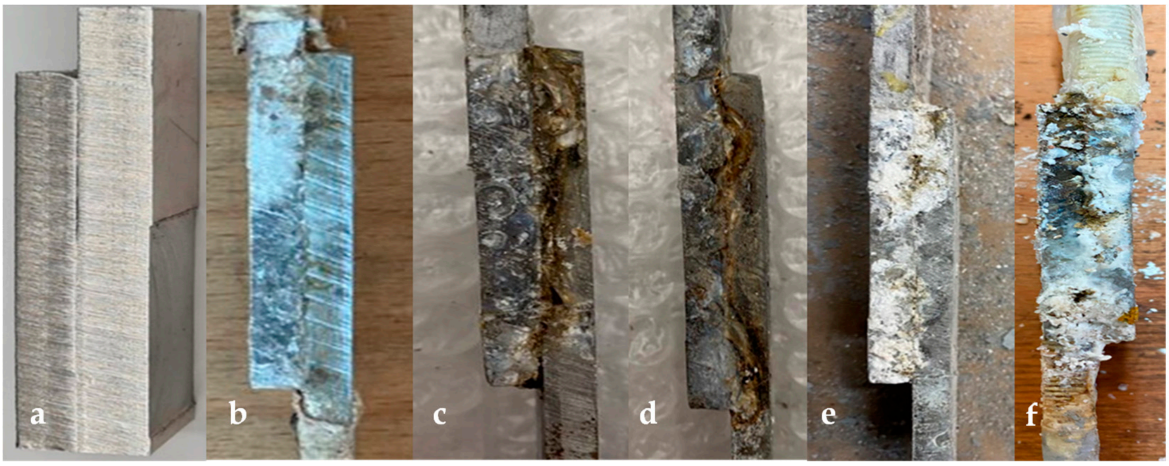

Figure 4. FSW advancing side at time (**a**) 0, (**b**) 2 months, (**c**) 4 months, (**d**) 6 months, (**e**) 8 months, and (**f**) 12 months.

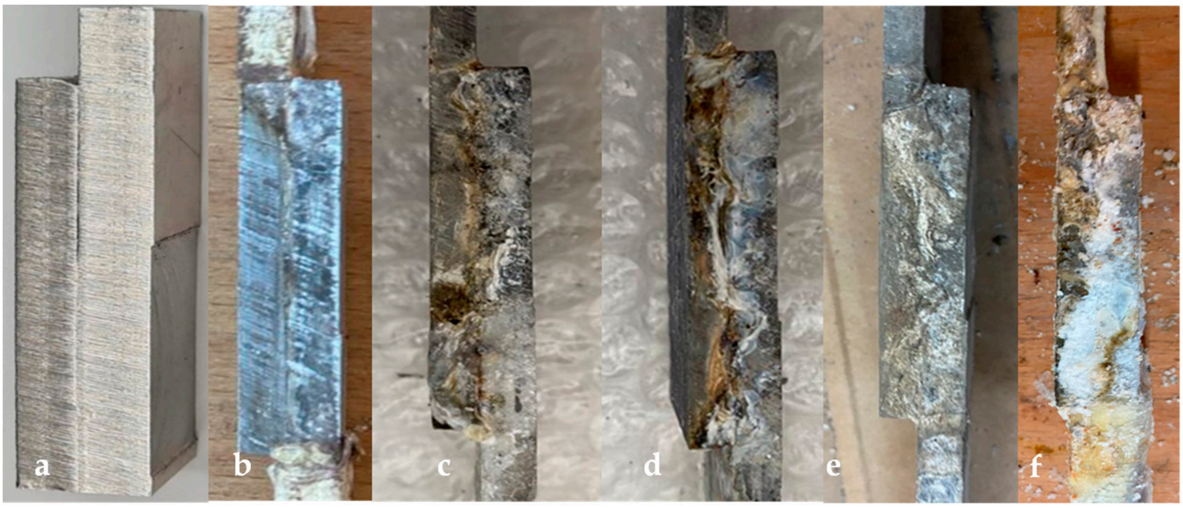

Figure 5. FSW retreating side at time (**a**) 0, (**b**) 2 months, (**c**) 4 months, (**d**) 6 months, (**e**) 8 months, and (**f**) 12 months.

The corrosion process is triggered and slowly proceeds over time without causing the joint to collapse. As time increases, it is interesting to note that the joints at the end of the experiment have limited corrosion at the interface. This means that the response of the joints was not homogeneous, and those that did not break during aging sometimes resisted while maintaining a high resistance value, comparable to the initial one at T0.

3.2. Tensile Test

Figure 6 reports load-displacement curves for three intermediate points of the investigated parameters, which constitute the most significant for the research. These are characterized by the same trend, and they are almost overlapping. For all the samples, the curve is characterized by two regions with different slopes. Firstly, the load slightly increases due to small settings in the areas around the weld. Then, the load sharply increases until it reaches the maximum value corresponding to the failure of the joint. The breakage abruptly occurs with the separation of the two welded sheets along the welding surface. As the aging time increases, the maximum load reached by the samples decreases.

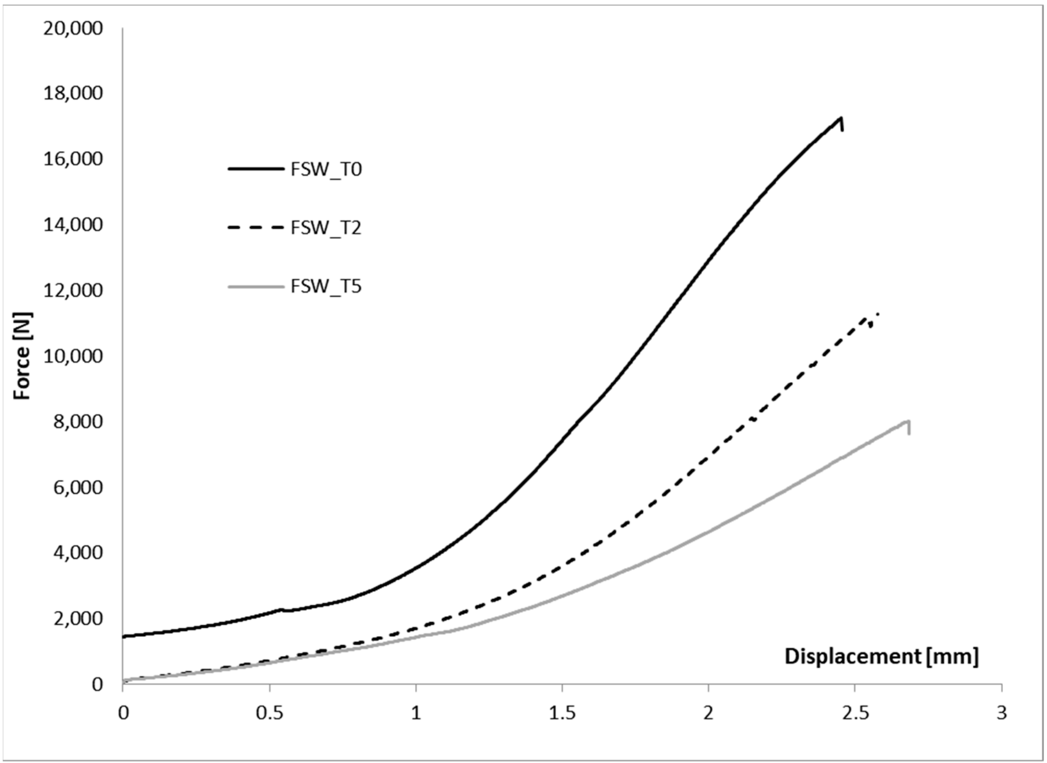

Figure 6. Typical displacement curves for advancing and retreating side joints at increasing ages.

4. Discussion

Figures 7–12 show the interfaces of the broken samples after the tensile test, produced on both the advancing and retreating sides and subjected to accelerated aging from time T0 to time T5. In the figures, only one sample for each combination of factors has been reported. However, the other four replicas are almost similar except for the samples that were already broken in the climate chamber. The results show, regardless of the welding direction, that the breakage occurs at the junction interface. A preliminary visual analysis shows that by increasing the time spent in the salt spray chamber, corrosion also increases.

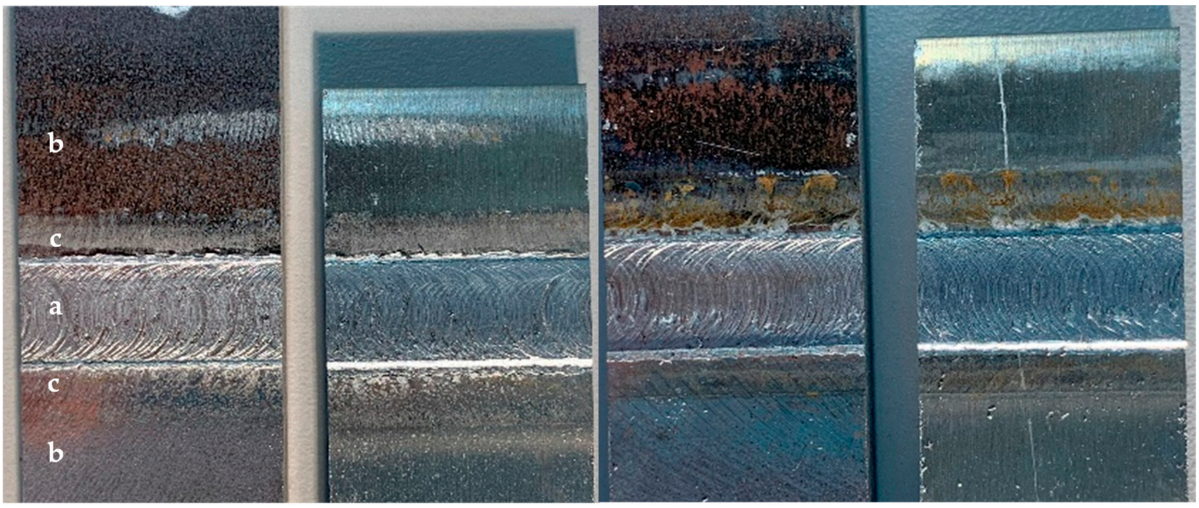

Figure 7. Fracture mode of FSW_AD and FSW_R samples at T0 ((**a**) mixing area, (**b**) free areas, (**c**) transition areas).

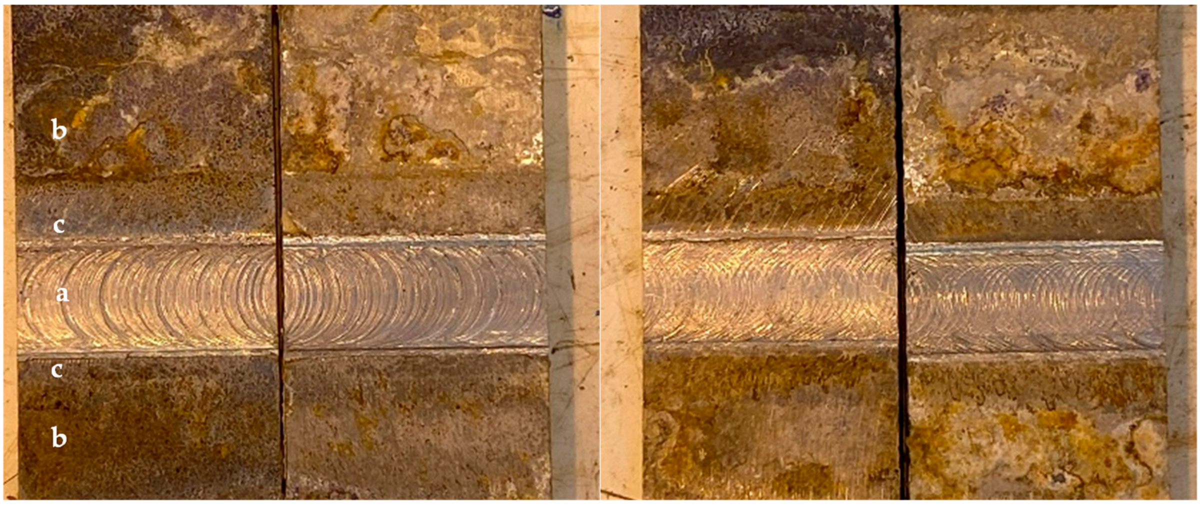

Figure 8. Fracture mode of FSW_AD and FSW_R samples at T1 ((**a**) mixing area, (**b**) free areas, (**c**) transition areas).

Figure 9. Fracture mode of FSW_AD and FSW_R samples at T2 ((**a**) mixing area, (**b**) free areas, (**c**) transition areas).

Figure 10. Fracture mode of FSW_AD and FSW_R samples at T3 ((**a**) mixing area, (**b**) free areas, (**c**) transition areas).

Figure 11. Fracture mode of FSW_AD and FSW_R samples at T4 ((**a**) mixing area, (**b**) free areas, (**c**) transition areas).

Figure 12. Fracture mode of FSW_AD and FSW_R samples at T5 ((**a**) mixing area, (**b**) free areas, (**c**) transition areas).

Particularly, it is possible to observe that:

1. There are no significant differences between advancing and retreating, in fact, the corrosion distribution is similar in both cases.
2. By increasing the exposition time, the products of corrosion affect the areas of the joint in different ways (i.e., Figure 8):
    a. The area of mixing where the welding occurs is clean, except at the time T3. Consequently, the joint maintains a good quality during its use. Then, the reduction of the resistance cannot be connected to the corrosion phenomena in this area.
    b. The free areas of aluminum and steel are covered by the products of corrosion.
    c. The areas between the free sheets and the mixing zone where the aluminum and steel are in intimate contact, but they are not joined, are clean, considering the low time of exposition. By increasing the time, the corrosion products penetrate these areas by promoting the opening of the joint. Consequently, the mechanical resistance is reduced by this action.

The performed experimental campaign was based on a Design of Experiment with two factors (namely Month and Welding direction), respectively, with 6 and 2 levels (namely T0–T5 and AD/R).

With the Minitab17® software, a variance analysis (ANOVA) was performed aiming to evaluate if the difference in mechanical properties ("maximum load" and "displacement at maximum load") between the joint realized in the advancing side or in the retreating side is significant, varying the aging time.

The whole experimental max load data are reported in Figure 13. In such a figure, the histogram is based on the mean values and the range of values that it contains. With a 95% probability, the true value of the max load is shown (interval plot with the confidence intervals estimated at 95%).

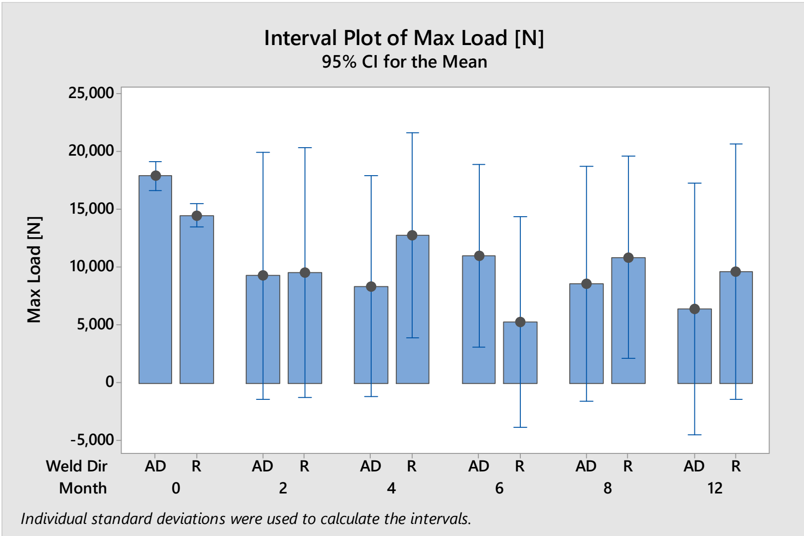

Figure 13. Maximum loads for AD/R joints at the five points of aging.

In Figure 14, the distribution of data and residuals was checked, showing a normal distribution and a random distribution of residuals versus fits. The purpose of this test is to ensure that the hypotheses for the ANOVA are respected. In the first plot, the data residuals are almost positioned in a straight line, which confirms that we can assume a normal distribution. The values of residuals, both versus fits and versus order, confirm the error's randomness. It is worth noting that the residual values are often very high because of the relevant spreading, which was already shown in the previous paragraph.

Table 4 summarizes the main results of the ANOVA by considering that one single parameter (i.e., maximum load) was investigated by varying it on two levels (i.e., the advancing and retreating sides).

Table 4. ANOVA: Analysis of variance for maximum load [N].

Analysis of Variance					
Source	**DF**	**Adj SS**	**Adj MS**	**F-Value**	***p*-Value**
Model	11	6,0742,7944	55,220,722	1.01	0.453
Linear	6	437,395,888	72,899,315	1.33	0.261
Weld Dir	1	1,840,592	1,840,592	0.03	0.855
Month	5	435,555,296	87,111,059	1.59	0.180
2-Way Interactions	5	170,032,056	34,006,411	0.62	0.684
Weld Dir*Month	5	170,032,056	34,006,411	0.62	0.684
Error	48	2,626,221,411	54,712,946		
Total	59	3,233,649,355			

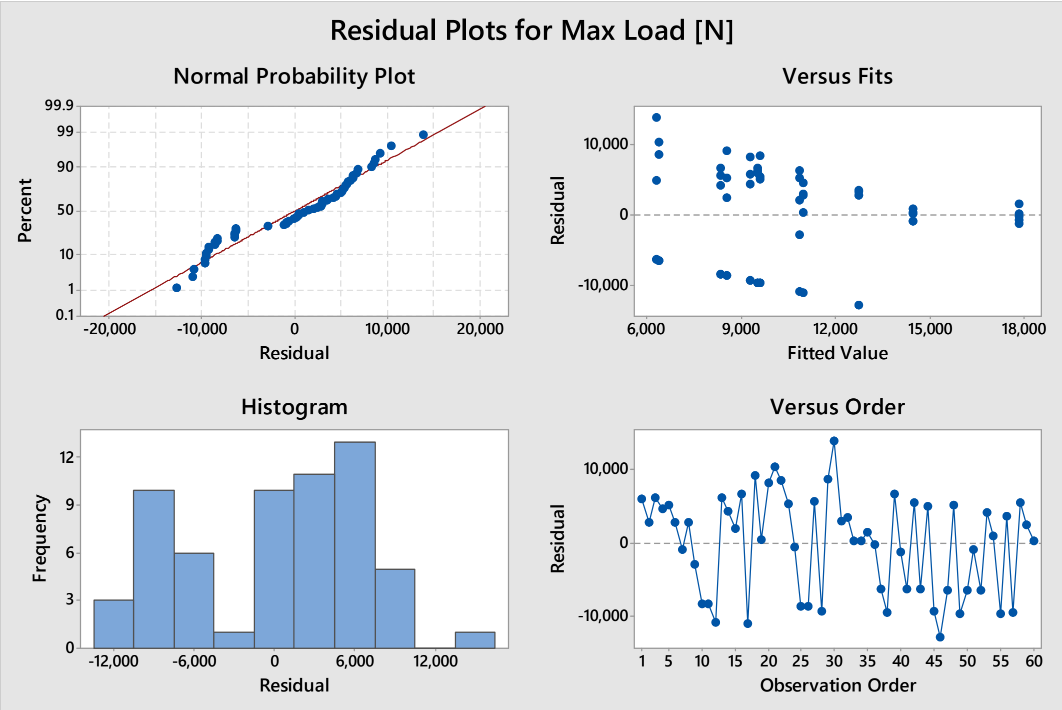

Figure 14. ANOVA–distribution of data and residual for Max Load.

DFs are the degrees of freedom, used to calculate the mean square (MS). In general, they measure how much 'independent' information is available to calculate each sum of squares (SS). This last, also called sum of the squared deviations, measures the total variability in the data, which is made up of the following sources: (i) the SS for each of the two factors, which measures how much the level means differ within each factor; (ii) the SS for the interaction, which measures how much the effects of one factor depend on the level of the other factor; and (iii) the SS for error, which measures the variability that remains after the factors and interactions are taken into account. MS is simply SS divided by the degrees of freedom. The MSs for error is an estimate of the variance in the data left over after the differences in the means were accounted for. F is used to determine the *p*-value (*p*) which defines if the effect for a term is significant, i.e., if *p* is less than or equal to a selected level (i.e., 0.05, corresponding to a 95% level of confidence), the effect for the term is significant.

Because the *p*-values are greater than any reasonable alpha level, evidence exists where the two predictors and their interactions have no significant effect on strength.

It is evident that the presence of broken samples, starting from two months of aging induces too high variances of data to let us test if the welding direction can affect the maximum load. At the same time, obviously, the presence of such samples is evidence that the aging time has a relevant effect on the load resistance. It is worth noting that when the data started to decrease in number, it became too small to perform statistical assessments.

The main effects of the plot for max load are reported in the Figure 15. With this, the general mean values of the load, for all the AD samples and all the R samples, regardless of the aging time (on the left), show how negligible the effect of the welding direction is, with respect to the variation of the mean values attained by increasing the aging time (on the right). As for the effect of aging time (regardless of the welding direction), it is interesting that even though the ANOVA is not significant for this factor, the mean values show a decreasing trend with a mean lower than 10 Kn (the overall mean of the experimental data), starting from the second month. It can be estimated that after the second month, the decrease is higher than 40% (starting from 16 Kn to 10 Kn, we obtained such a value).

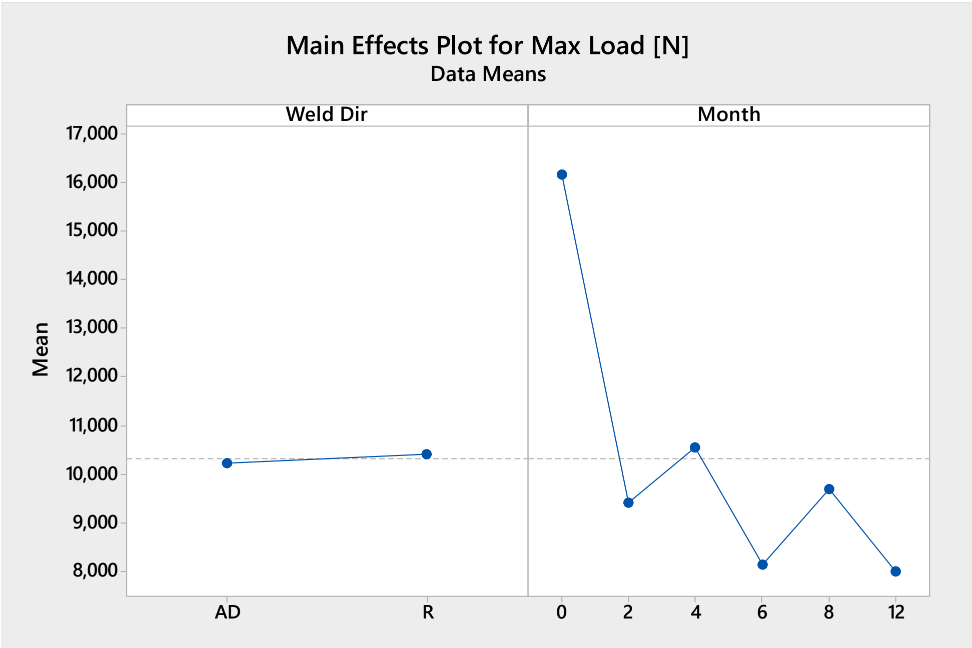

Figure 15. Main effects plot for max load.

Due to the relevant changes in the load data, with increasing time to inquire whether the welding direction has an influence on the maximum load or not on the tested samples, both one-way ANOVA and the Tukey pairwise comparison test for means have been performed on the data of each aging point not considering the broken samples. In the following, the results of the one-way ANOVA are summarized for the six different aging times. The data at T0 were already reported in a previous study [24].

In Figure 16, the Interval Plots of the max load data are reported for each aging time. In these figures, the max load data have lower ranges than in the previous analysis (see Figure 13). This is due to the fact that the broken samples are not taken into account in this case. Instead, the value zero for the broken samples caused the confidence intervals to be larger than the entire length of the histogram bars in Figure 13.

In these last diagrams, it is evident how the data ranges overlap each other, except at T0. The intervals that include the mean values are sometimes very similar, like at month 8, so the two populations, AD and R, are practically indistinguishable. In the other cases (see month 2 for examples), one is much larger than the other (in this case, the AD is much larger than R) including all the values of the second group. Even in these cases, it is not possible to distinguish one population from the other.

In Table 5, the one-way ANOVAs are summarized. The table shows the *p*-value calculated for each aging time and assesses if the factor "welding direction" induces a difference in the max load obtained from the tensile tests. From these results, it is evident that the value of probability is less than the value of 0.05 only at T0. So, we can conclude that during the aging period, the difference induced by the welding direction on the max load does not exist and it is overcome by the effect of aging.

Table 5. One-way ANOVA for maximum load [N].

	Source	DF	Adj SS	Adj MS	F	*p*
T0	Side	1	28,848,08	28,848,087	33.81	0.000
	Error	8	6,826,656	853,332		
	Total	9	35,674,743			
	S = 923.760		R-Sq = 80.86%		R-Sq(adj) = 78.47%	
	Source	DF	Adj SS	Adj MS	F	*p*
T1	Side	1	272,147	272,147	0.14	0.730
	Error	4	7,934,991	1,983,748		
	Total	5	8,207,138			
	S = 1408.46		R-Sq = 3.32%		R-Sq(adj) = 0%	
	Source	DF	Adj SS	Adj MS	F	*p*
T2	Side	1	7,023,319	7,023,319	7.55	0.052
	Error	4	3,721,521	930,380		
	Total	5	10,744,840			
	S = 964.562		R-Sq = 65.36%		R-Sq(adj) = 56.71%	
	Source	DF	Adj SS	Adj MS	F	*p*
T3	Side	1	5,361,918	5,361,918	0.44	0.545
	Error	4	49,135,572	12,283,893		
	Total	5	54,497,490			
	S = 3504.84		R-Sq = 9.84%		R-Sq(adj) = 0%	
	Source	DF	Adj SS	Adj MS	F	*p*
T4	Side	1	772,141	772,141	0.05	0.828
	Error	5	74,005,944	14,801,189		
	Total	6	74,778,085			
	S = 3847.23		R-Sq = 0%		R-Sq(adj) = 0%	
	Source	DF	Adj SS	Adj MS	F	*p*
T5	Side	1	1,332,801	1,332,801	0.56	0.509
	Error	3	7,140,065	2,380,022		
	Total	4	8,472,866			
	S = 1542.73		R-Sq = 15.73%		R-Sq(adj) = 0%	

The Tukey pairwise comparison results are reported in Figure 17. They confirm that only the difference in the mean of the max load at T0 between the retreating and advancing sides is significant.

This test compares the means of every treatment to the means of every other treatment. In particular, it applies simultaneously to the set of all pairwise comparisons, R-AD, and identifies any difference between the two means that are greater than the expected standard error. In the graphical representation reported below, if the interval (which represents the difference between the two means R-AD) does not contain zero, then they are significantly different.

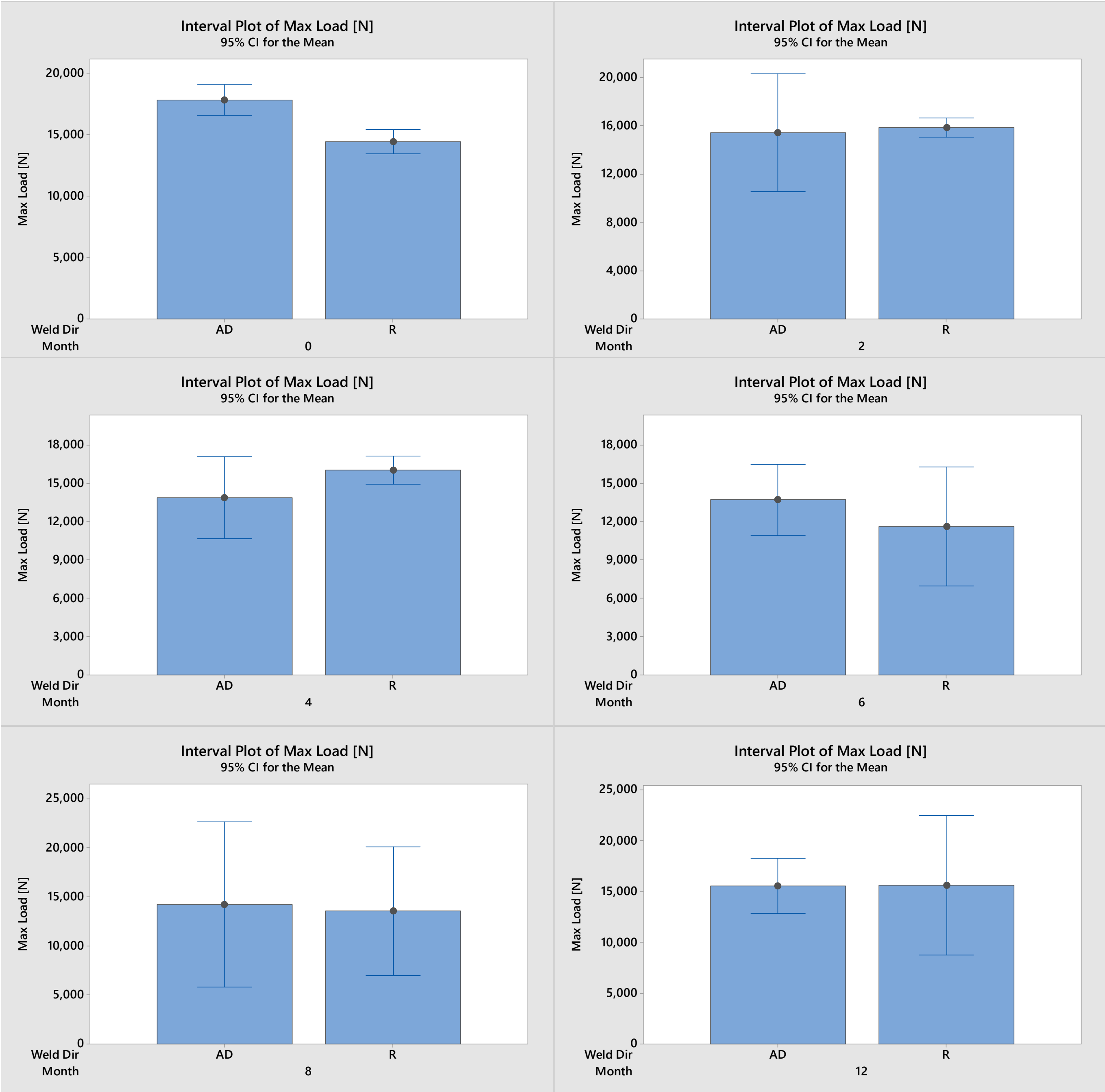

Figure 16. Interval plot of max load.

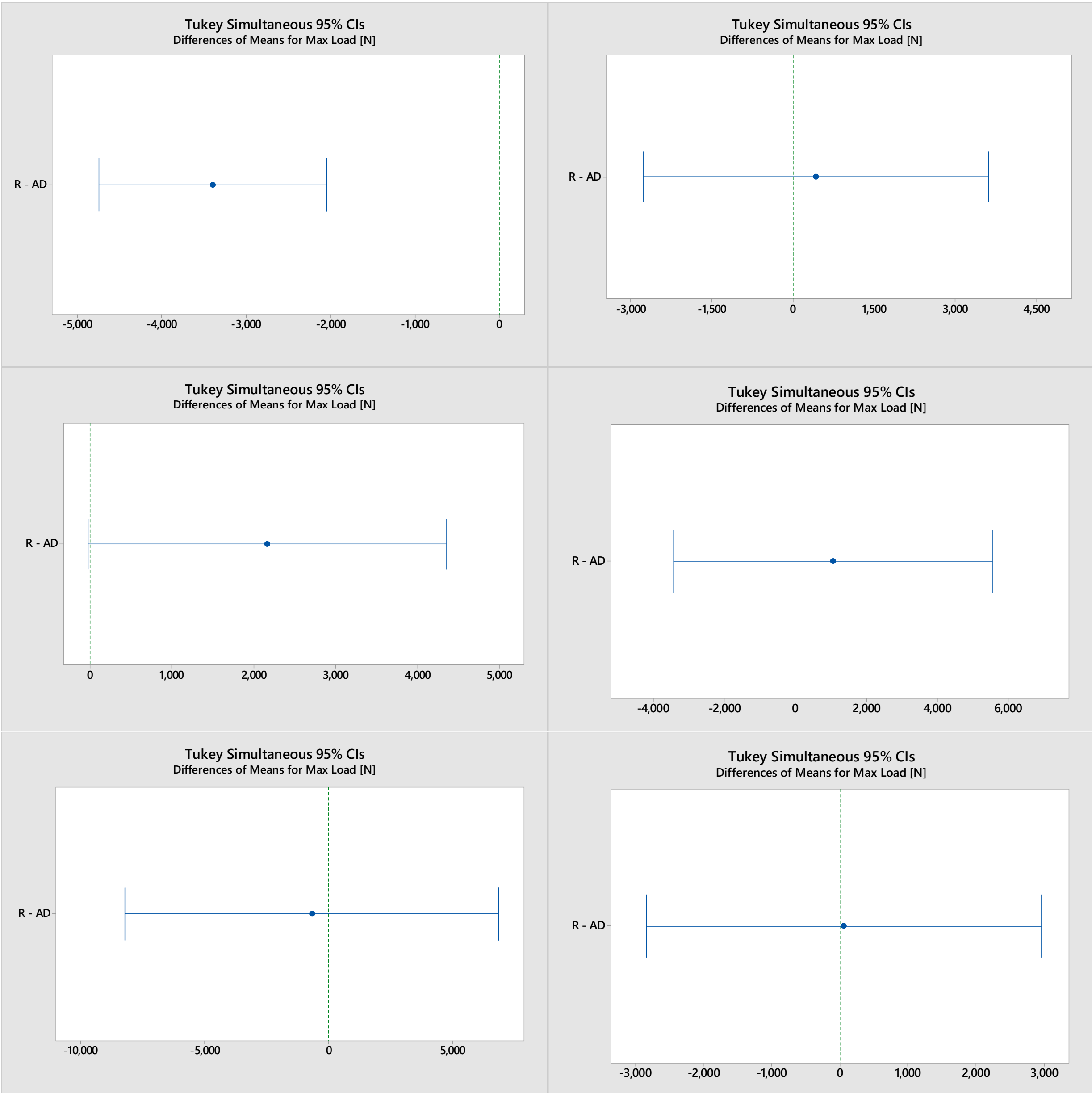

Figure 17. Tukey pairwise comparisons for the six aging times (from top left to bottom right: 0, 2, 4, 6, 8, 12 months).

ANOVA: Analysis of Variance for Displacement at Maximum Load [mm]

The whole data of displacement at max load are summarized in Figure 18. It is possible to observe how by increasing the aging time, the spreading of data increases. As for the max load data, the presence of the value zero, due to the existence of the specimens that were broken before the execution of the test in the climate chamber, causes an increase in the spreading. The reason this spread is lower than the load data of Figure 13 is that the displacement data has a smaller absolute value, which is much closer to zero.

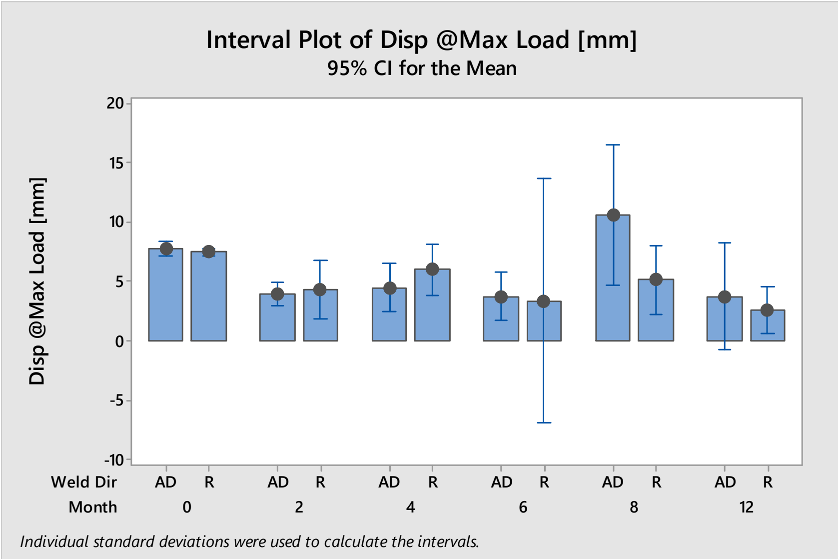

Figure 18. Displacement at maximum loads for AD/R joints at the five points of aging.

In Figure 19, the distribution of data and residuals was checked, showing a normal distribution and a random distribution of residuals versus fits.

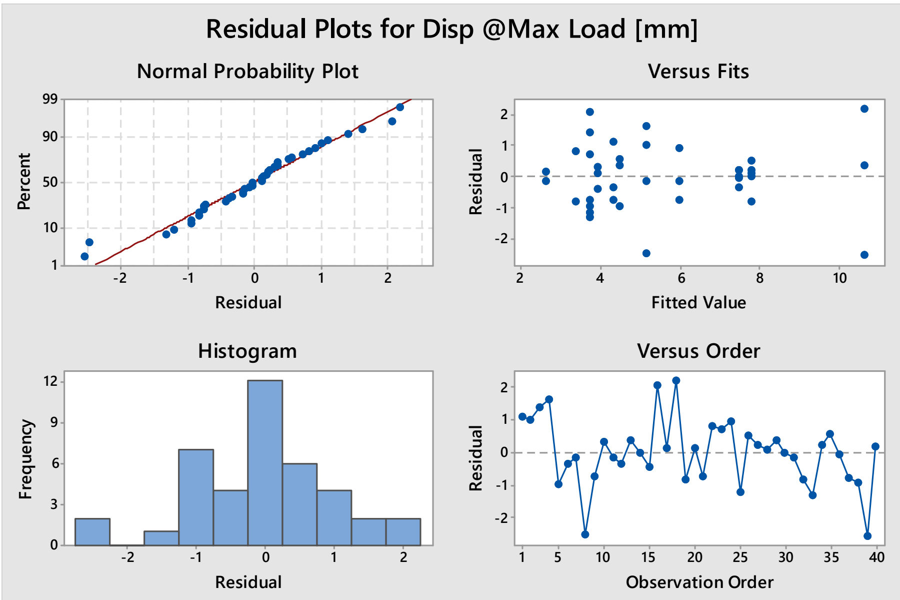

Figure 19. ANOVA–distribution of data and residual for Displacement at Max Load.

Table 6 summarizes the main results of the variance analysis by considering that one single parameter (i.e., displacement at max load) was investigated by varying the two levels (i.e., the advancing and retreating sides).

Because the *p*-values are lower than the fixed alpha level, 0.05, evidence exists that the two predictors and their interaction have a significant effect on the displacement at max load.

The main effects plot for displacement at max load is reported in Figure 20. With this, the general mean values of load, for all the AD samples and all the R samples regardless of the aging time, show how negligible the effect is with respect to the variation of the mean values attained by increasing the aging time.

Table 6. ANOVA: Analysis of variance for displacement at maximum load [N].

Analysis of Variance					
Source	**DF**	**Adj SS**	**Adj MS**	**F-Value**	***p*-Value**
Model	11	187.275	17.025	11.82	0.000
Linear	6	142.626	23.771	16.50	0.000
Weld Dir	1	7.426	7.426	5.15	0.031
Month	5	141.166	28.233	19.60	0.000
2-Way Interactions	5	48.276	9.655	6.70	0.000
Weld Dir*Month	5	48.276	9.655	6.70	0.000
Error	28	40.340	1.441		
Total	39	227.616			

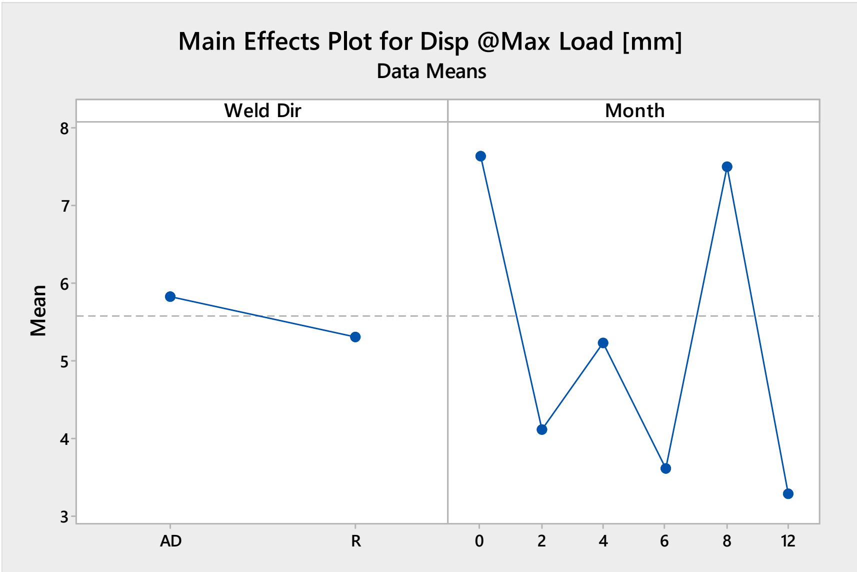

Figure 20. Main effects plot for displacement at max load.

From this figure, it is possible to affirm that the AD samples exhibit slightly higher displacement before reaching the max load. Such a difference in the whole data is in the order of less than one millimeter. As for the effect of aging, the data show a decrease of mean displacement all along the aging time, except for the data at month 8 where higher values are shown. This fact could be related to the presence of corrosion products. The very high data spreading and the low number of specimens, increasing aging time, do not allow to us assess the relevant results.

To consider the incidence of the number of broken specimens during aging, this number has been divided by the total number of specimens for each welding direction and for each aging time. The results are shown in Figure 21.

For the number of studied specimens, no difference between the two welding directions was found. Moreover, it is worth noticing that starting from the second month, the effect of corrosion leads to excessive damage to the welding that is almost stationary until the 12th month when half of the population of samples is completely damaged.

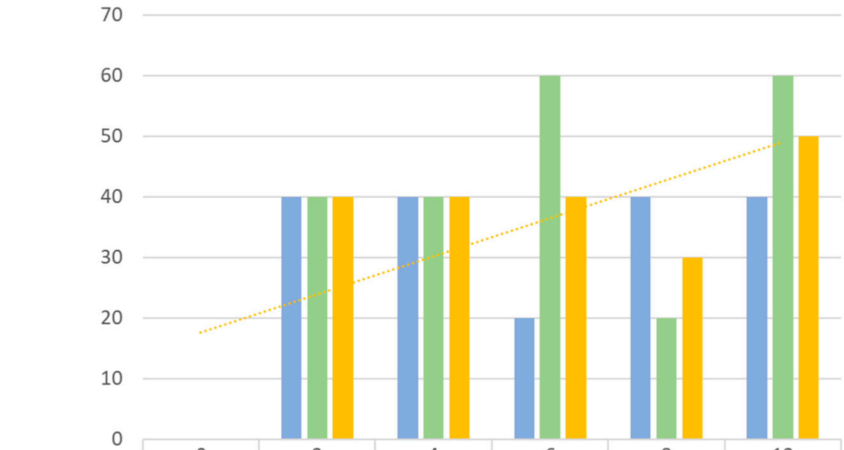

	0	2	4	6	8	12
% failure AD	0	40	40	20	40	40
% failure R	0	40	40	60	20	60
% total	0	40	40	40	30	50

Figure 21. Percentage of broken specimens at varying aging times.

5. Conclusions

In this study, FSW joints between steel and aluminum alloys have been subjected to accelerated aging tests. In the first part of the work, data resulting from tensile tests are reported and a preliminary analysis of the aging process is obtained. The main results can be summarized as follows:

The breakage of the samples during the tensile tests occurs always at the junction interface. The surfaces of fracture do not evidence significant differences with changing welding direction (see Figures 8–12).

By increasing the exposure time, the products of corrosion affect the surface of the fractures in the following ways: The area of mixing where welding occurs is clean. The free areas of aluminum and steel are covered by the products of corrosion. The areas between the free sheets and the mixing zone, where the aluminum and steel are in intimate contact (but are not joined) are clean for a low time of exposure, but the corrosion products penetrate for a high exposure time by promoting the failure of the joint.

Moreover, according to the statistical analysis of the data:

- Between the investigated factors (welding direction and aging time), the welding direction influences the mechanical resistance of the joints only if they are not subjected to a salt fog test. The advancing side joints are characterized by a higher joint strength compared with the retreating side ones at T0, while no significant difference in max load is recorded during the first year of aging.
- The aging time severely influences the joint resistance starting from the first point of the test (i.e., 2 months). Starting from the first point of aging, the maximum load decreases by about 40%, and some specimens are already broken in the salt spray chamber.
- The data of displacement at max load obtained by the tensile are very scattered when increasing the aging time. This fact, together with the low number of samples tested at high aging time, does not allow us to assess any relevant result.

As for the specimens broken before the tensile test, by increasing aging time, no difference between the two welding directions is found. Moreover, it is worth noticing that starting from the second month, the effect of corrosion leads to excessive damage to the welding, which is almost stationary until the 12th month when half of the population of samples is damaged.

All the tested joints, at different aging times, will undergo further tests (microhardness and metallographic analysis) with the aim of focusing on how the corrosion phenomena occur.

Author Contributions: Conceptualization, G.D.B., B.C. and F.F.; methodology, G.D.B., B.C. and F.F.; formal analysis, B.C. and F.F.; investigation, G.D.B., B.C. and F.F.; resources, B.C.; data curation, F.F.; writing—original draft preparation, F.F. and B.C.; writing—review and editing, B.C. and F.F.; visualization, G.D.B.; supervision, B.C.; project administration, G.D.B. and B.C. All authors have read and agreed to the published version of the manuscript.

Funding: This research was funded by Sicilian Region on the European Regional Development Fund 2014–2020, as part of the project "Innovative Solutions for High Energy Saving Naval Vessels (SI-MARE)", grant number 08ME7219090182.

Data Availability Statement: Data are contained within this article.

Conflicts of Interest: The authors declare no conflicts of interest. The funders had no role in the design of the study; in the collection, analyses, or interpretation of data; in the writing of the manuscript; or in the decision to publish the results.

References

1. Cischino, E.; Vulugu, Z.; Ezeiza, C.E.; Benito, I.L.; Mangino, E.; Cristiansen, J.C.; Sanporean, C.G.; Paolo, F.; Kirpluks, M.; Cabulis, P. A concrete and viable example of multi-material body: The Evolution project main outcomes. *Proceedia CIRP* **2017**, *66*, 300–305. [CrossRef]
2. Gullino, A.; Matteis, P.; D'Aiuto, F. Review of aluminium to steel welding technologies for car-body applications. *Metals* **2019**, *9*, 315. [CrossRef]
3. Panayotova, M.; Garbatov, Y.; Soares, C.G. *Corrosion of Steels in Marine Environment, Monitoring and Standards, Safety and Reliability of Industrial Products, Systems and Structures*; Taylor & Francis Group: Abingdon, UK, 2008; pp. 369–412.
4. Le Bozec, N.; Le Gac, A.; Thierry, D. Corrosion performance and mechanical properties of joined automotive materials. *Mater Corros.* **2012**, *63*, 408–415. [CrossRef]
5. Zhang, C.; Cao, Y.; Huang, G.; Zeng, Q.; Zhu, Y.; Huang, X.; Liu, Q. Influence of tool rotational speed on local microstructure, mechanical and corrosion behavior of dissimilar AA2024/7075 joints fabricated by friction stir welding. *J. Manuf. Process.* **2020**, *49*, 214–226. [CrossRef]
6. Shankar, S.; Mehta, K.P.; Chattopadhyaya, S.; Vilaça, P. Dissimilar friction stir welding of Al to non-Al metallic materials: An overview. *Mater. Chem. Phys.* **2022**, *288*, 126371. [CrossRef]
7. Sahu, M.; Ganguly, S. Distribution of intermetallic compounds in dissimilar joint interface of AA 5083 and HSLA steel welded by FSW technique. *Intermetallics* **2022**, *151*, 107734. [CrossRef]
8. Du, Z.; Chen, H.-C.; Tan, M.J.; Bi, G.; Chua, C.K. Investigation of Porosity Reduction, Microstructure and Mechanical Properties for Joining of Selective Laser Melting Fabricated Aluminium Composite Via Friction Stir Welding. *J. Manuf. Process.* **2018**, *36*, 33–43. [CrossRef]
9. Steenbergen, J.E.; Thornton, H.R. Quantitative determination of the conditions for hot cracking during welding of aluminium alloys. *Weld. J.* **1970**, *49*, 61s–68s.
10. Heidarzadeh, A.; Mironov, S.; Kaibyshev, R.; Çam, G.; Simar, A.; Gerlich, A.; Khodabakhshi, F.; Mostafaei, A.; Field, D.P.; Robson, J.D.; et al. Friction stir welding/processing of metals and alloys: A comprehensive review on microstructural evolution. *Prog. Mater. Sci.* **2021**, *117*, 100752. [CrossRef]
11. Chen, Z.W.; Yazdanian, S.; Littlefair, G. Effects of tool positioning on joint interface microstructure and fracture strength of friction stir lap Al-to-steel welds. *J. Mater. Sci.* **2013**, *48*, 2624–2634. [CrossRef]
12. Mortello, M.; Pedemonte, M.; Contuzzi, N.; Casalino, G. Experimental Investigation of Material Properties in FSW Dissimilar Aluminum-Steel Lap Joints. *Metals* **2021**, *11*, 1474. [CrossRef]
13. Raj, S.; Biswas, P. Experimental investigation of the effect of induction preheating on the microstructure evolution and corrosion behaviour of dissimilar FSW (IN718 and SS316L) joints. *J. Manuf. Process.* **2023**, *95*, 143–159. [CrossRef]
14. Palanivel, R.; Koshy Mathews, P.; Murugan, N. Optimization of process parameters to maximize ultimate tensile strength of friction stir welded dissimilar aluminum alloys using response surface methodology. *J. Cent. South Univ.* **2013**, *20*, 2929–2938. [CrossRef]
15. Kasman, S.; Kahraman, F.; Emiralioğlu, A.; Kahraman, H. A Case Study for the Welding of Dissimilar EN AW6082 and EN AW 5083 Aluminum Alloys by Friction StirWelding. *Metals* **2016**, *7*, 6. [CrossRef]
16. Jaia, S.; Sharmab, N.; Guptac, R. Dissimilar alloys (AA6082/AA5083) joining by FSW and parametric optimization using Taguchi, grey relational and weight method. *Eng. Solid Mech.* **2018**, *6*, 53–66.
17. Di Bella, G.; Alderucci, T.; Favaloro, F.; Borsellino, C. Effect of tool tilt angle on mechanical resistance of AA6082/AA5083 friction stir welded joints for marine applications. In Proceedings of the 16th CIRP Conference on Intelligent Computation in Manufacturing Engineering (CIRP ICME 2022), Naples, Italy, 13–15 July 2022.
18. Wloka, J.; Laukant, H.; Glatzel, U. Virtanen Corrosion properties of laser beam joints of aluminium with zinc-coated steel. *Corros. Sci.* **2007**, *49*, 4243–4258. [CrossRef]

19. Narsimhachary, D.; Rai, P.K.; Shariff, S.M.; Padmanabham, G.; Mondal, K.; Basu, A. Corrosion behavior of laser-brazed surface made by joining of AA6082 and galvanized steel. *J. Mater. Eng. Perform.* **2019**, *28*, 2115–2127. [CrossRef]
20. Calabrese, L.; Bonaccorsi, L.; Proverbio, E.; Di Bella, G.; Borsellino, C. Durability on alternate immersion test of self-piercing riveting aluminium joint. *Mater. Des.* **2013**, *46*, 849–856. [CrossRef]
21. Lim, Y.C.; Squires, L.; Pan, T.Y.; Miles, M.; Song, G.L.; Wang, Y.; Feng, Z. Study of mechanical joint strength of aluminum alloy 7075-T6 and dual phase steel 980 welded by friction bit joining and weld-bonding under corrosion medium. *Mater. Des.* **2015**, *69*, 37–43. [CrossRef]
22. Kulkarni, B.; Pankade, S.; Tayde, S.; Bhosle, S. Corrosion and Mechanical Aspects of Friction Stir Welded AA6061 Joints: Effects of Different Backing Plates. *J. Mater. Eng. Perform.* **2023**, *32*, 10817–10833. [CrossRef]
23. Anaman, S.Y.; Cho, H.-H.; Das, H.; Lee, J.-S.; Hong, S.-T. Microstructure and mechanical/electrochemical properties of friction stir butt welded joint of dissimilar aluminum and steel alloys. *Mater Charact.* **2019**, *154*, 67–79. [CrossRef]
24. Guido, D.B.; Chiara, B.; Amani, K.; Edoardo, P. Effect of tool rotation direction on mechanical strength of single lap Friction Stir Welded joints between AA5083 aluminum alloy and S355J0 steel for maritime applications. *Metals* **2023**, *13*, 411.
25. Khaskhoussi, A.; Di Bella, G.; Borsellino, C.; Calabrese, L.; Proverbio, E. Microstructural and electrochemical characterization of dissimilar joints of aluminum alloy AW5083 and carbon steel S355 obtained by friction welding. *Ital. Metall.* **2022**, *9*, 15–21.
26. *ASTM B117: 2018*; Standard Practice for Operating Salt Spray (Fog) Apparatus. Available online: https://www.astm.org/Standards/B117 (accessed on 8 July 2019).
27. *ISO 9227*; Corrosion Tests in Artificial Atmospheres—Salt Spray Tests. ISO: Geneva, Switzerland, 2017.
28. *UNI EN ISO 12996*; Destructive Testing of Joints—Specimen Dimensions and Test Procedure for Tensile Shear Testing of Single Joints. ISO: Geneva, Switzerland, 2013.